Enzymology:

Crystal Structure of the Ectoine Hydroxylase, a Snapshot of the Active Site

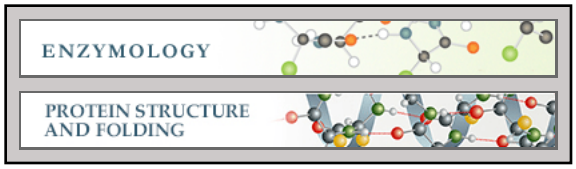

Astrid Höppner, Nils Widderich, Michael Lenders, Erhard Bremer and Sander H. J. Smits

J. Biol. Chem. 2014, 289:29570-29583.
doi: 10.1074/jbc.M114.576769 originally published online August 29, 2014

THE JOURNAL OF BIOLOGICAL CHEMISTRY VOL. 289, NO. 43, pp. 29570–29583, October 24, 2014

Crystal Structure of the Ectoine Hydroxylase, a Snapshot of the Active Site*

Received for publication, April 25, 2014, and in revised form, August 27, 2014 Published, JBC Papers in Press, August 29, 2014, DOI 10.1074/jbc.M114.576769

Astrid Höppner[‡1], **Nils Widderich**[§¶1,2], **Michael Lenders**[‖], **Erhard Bremer**[§**3], **and Sander H. J. Smits**[‖4]

From the [‡]*X-ray Facility and Crystal Farm, Heinrich-Heine-University at Düsseldorf, D-40225 Düsseldorf, the* [§]*Department of Biology, Laboratory for Microbiology, Philipps-University at Marburg, D-35043 Marburg, the* [¶]*Max Planck Institute for Terrestrial Microbiology, Emeritus Group R. K. Thauer, D-35043 Marburg, the* [‖]*Institute of Biochemistry, Heinrich-Heine-University at Düsseldorf, D-40225 Düsseldorf, and the* **LOEWE-Center for Synthetic Microbiology, Philipps-University at Marburg, D-35043 Marburg, Germany*

Background: 5-Hydroxyectoine is a compatible solute synthesized by the ectoine hydroxylase (EctD), a non-heme containing iron(II) and 2-oxoglutarate-dependent dioxygenase.
Results: The structure of EctD was solved in different forms.
Conclusion: The architecture of the catalytic core of EctD was revealed.
Significance: The crystal structure increases our understanding of the structural-functional relationship in an evolutionary conserved group of enzymes.

Ectoine and its derivative 5-hydroxyectoine are compatible solutes that are widely synthesized by bacteria to cope physiologically with osmotic stress. They also serve as chemical chaperones and maintain the functionality of macromolecules. 5-Hydroxyectoine is produced from ectoine through a stereo-specific hydroxylation, an enzymatic reaction catalyzed by the ectoine hydroxylase (EctD). The EctD protein is a member of the non-heme-containing iron(II) and 2-oxoglutarate-dependent dioxygenase superfamily and is evolutionarily well conserved. We studied the ectoine hydroxylase from the cold-adapted marine ultra-microbacterium *Sphingopyxis alaskensis* (*Sa*) and found that the purified *Sa*EctD protein is a homodimer in solution. We determined the *Sa*EctD crystal structure in its apo-form, complexed with the iron catalyst, and in a form that contained iron, the co-substrate 2-oxoglutarate, and the reaction product of EctD, 5-hydroxyectoine. The iron and 2-oxoglutarate ligands are bound within the EctD active site in a fashion similar to that found in other members of the dioxygenase superfamily. 5-Hydroxyectoine, however, is coordinated by EctD in manner different from that found in high affinity solute receptor proteins operating in conjunction with microbial import systems for ectoines. Our crystallographic analysis provides a detailed view into the active site of the ectoine hydroxylase and exposes an intricate network of interactions between the enzyme and its ligands that collectively ensure the hydroxylation of the ectoine substrate in a position- and stereo-specific manner.

Cells of all three kingdoms of life exploit compatible solutes as protectants against water loss that ensues upon their exposure to high osmolarity surroundings (1, 2). These organic compounds can be accumulated to exceedingly high intracellular concentrations without exerting negative side effects on the biochemistry of the cell. They thus serve as physiologically compliant water-attracting osmolytes to maintain an adequate level of cellular hydration (3). The physicochemical attributes of compatible solutes that make their physiological function(s) possible largely stem from their negative interactions with the protein backbone that in turn leads to their preferential exclusion from protein surfaces (4). As a consequence of the resulting imbalance of the distribution of compatible solutes in the cell water, thermodynamics favor the native conformation of proteins and the functionality of other macromolecules under otherwise function-disrupting conditions (5, 6). The term "chemical chaperone" has been coined in the literature to reflect these beneficial traits (7).

Ectoine ((4*S*)-2-methyl-1,4,5,6-tetrahydropyrimidine-4-carboxylic acid) (Fig. 1) (8) is a well recognized compatible solute and microbial stress protectant (9, 10). Its function-preserving (10–15) and anti-inflammatory properties fostered substantial interest for its industrial scale production (9, 16) and exploitation in various biotechnological applications, in skin-care products (9, 10, 16–18), and in potential medical uses (19–21). Ectoine is synthesized widely by members of bacteria (10, 16, 22) as an adaptive response to osmotic stress (16, 23–29) and growth-restricting extremes in high and low temperatures (25, 30). Synthesis of ectoine relies on the supply of the precursor L-aspartate-β-semialdehyde and is carried out through the enzymatic

* This work was supported in part by Deutsche Forschungsgemeinschaft Grant SFB 987, the LOEWE program of the State of Hessen (via the Center for Synthetic Microbiology, Marburg), the Max-Planck Institute for Terrestrial Microbiology (Marburg) through the Emeritus Group of R. K. Thauer, a contribution by the Fonds der Chemischen Industrie, by the Heinrich-Heine-University Düsseldorf and its Institute of Biochemistry, and by the initiative "Fit for Excellence" of the Heinrich-Heine-University.
The atomic coordinates and structure factors (codes 4Q5O, 4MHR, and 4MHU) have been deposited in the Protein Data Bank (http://wwpdb.org/).
[1] Both authors contributed equally to this work.
[2] Recipient of a Ph.D. fellowship from the International Max Planck Research School for Environmental, Cellular, and Molecular Microbiology, Marburg, Germany.
[3] To whom correspondence may be addressed: Philipps-University Marburg, Karl-von-Frisch Str. 8, D-35043 Marburg, Germany. Tel.: 49-6421-282-1529; Fax: 49-6421-282-8979; E-mail: bremer@staff.uni-marburg.de.
[4] To whom correspondence may be addressed: Heinrich-Heine-University, Institute of Biochemistry, Universitätsstr. 1, D-40225 Düsseldorf, Germany. Tel.: 49-2118112647; Fax: 49-211-8115310; E-mail: Sander.Smits@hhu.de.

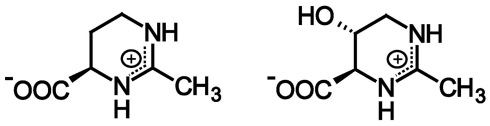

ectoine 5-hydroxyectoine

FIGURE 1. **Chemical structures of ectoine and 5-hydroxyectoine.**

activities of L-2,4-diaminobutyrate transaminase (EctB; EC 2.6.1.76), 2,4-diaminobutyrate acetyltransferase (EctA; EC 2.3.1.178), and ectoine synthase (EctC; EC 4.2.1.108) (22, 31, 32).

A substantial group of ectoine producers (22) also synthesize a derivative in which a hydroxy group is attached to the pro-*S* hydrogen at position C5 in the tetrahydropyrimidine ring of ectoine in a stereo-specific manner, thereby yielding 5-hydroxyectoine ((4*S*,5*S*)-5-hydroxy-2-methyl-1,4,5,6-tetrahydropyrimidine-4-carboxylic acid (Fig. 1) (33), a reaction carried out by the ectoine hydroxylase (EctD; EC 1.14.11) (27, 30, 34). Despite their closely related chemical structures, 5-hydroxyectoine is often superior to its precursor molecule ectoine in protecting microorganisms against environmentally imposed stresses (26, 30) and in preserving the functionality of macromolecules and cells (11–15, 35, 36). This makes a better understanding of the ectoine hydroxylase desirable, both in terms of basic science and for its practical use in biotechnological processes.

The ectoine hydroxylase is a member of the non-heme-containing iron(II) and 2-oxoglutarate-dependent dioxygenase superfamily, a group of versatile biocatalysts that not only carry out hydroxylation reactions but also dimethylations, desaturations, cyclizations, ring expansions, epimerizations, and halogenations (37–41). Although the type of substrates used by these dioxygenases varies considerably, common enzyme reaction mechanisms are observed. Most members of this superfamily couple the two-electron oxidation of their substrates with the reaction of oxygen and 2-oxoglutarate (38, 39, 42). The ectoine hydroxylase adheres to this general reaction scheme (27, 43).

Despite their varied enzyme activities, non-heme-containing iron(II) and 2-oxoglutarate-dependent dioxygenases are structurally closely related and typically consist of a double-stranded β-helix (DSBH)[5] core, the so-called jelly roll or cupin fold (37–40). Crystallographic analysis of the ectoine hydroxylase from the salt-tolerant moderate halophile *Virgibacillus salexigens* (*Vs*) in its iron-bound (44) and iron-free (22) forms revealed that the DSBH in the *Vs*EctD protein is formed by four-stranded antiparallel β-sheets arranged in form of a β-sandwich; it is decorated with and stabilized by a number of α-helices (22, 44). However, both available crystal structures of the *Vs*EctD protein lack the co-substrate 2-oxoglutarate and the substrate ectoine, and consequently, our understanding of the structure and architecture of the active site of this enzyme is incomplete.

[5] The abbreviations used are: DSBH, double-stranded β-helix; r.m.s.d., root mean square deviation; ASU, asymmetric unit; TES, 2-{[2-hydroxy-1,1-bis(hydroxymethyl)ethyl]amino}ethanesulfonic acid; PDB, Protein Data Bank; MALS, multiangle light scattering.

Recently, we have biochemically characterized six ectoine hydroxylases from microorganisms that are able to colonize habitats with extremes in salinity, growth temperature, and pH values (22). These six enzymes possess kinetic parameters similar to those of the previously studied ectoine hydroxylases from *V. salexigens* and *Streptomyces coelicolor* (26, 27), but differences in their ability to withstand the inhibiting effects of high salt concentrations and high temperature were noted for some of them (22). These enzymes might thus be better suited than the *V. salexigens* EctD protein to obtain a crystal structure containing all ligands.

Here, we report the crystal structures of the ectoine hydroxylase from the cold-adapted marine ultra-microbacterium *Sphingopyxis alaskensis* (45), *Sa*EctD (22, 46), in its apo-form, in complex with iron and in a form that contains the iron catalyst, the co-substrate 2-oxoglutarate and the product of the EctD-catalyzed enzyme reaction, 5-hydroxyectoine. Combined with previous molecular dynamics simulations (44), the crystallographic analysis presented here and our site-directed mutagenesis experiments revealed the architecture of the active site of this evolutionarily well conserved group of enzyme.

EXPERIMENTAL PROCEDURES

Chemicals—Ectoine and 5-hydroxyectoine were kindly provided by Dr. Thomas Lentzen and Dr. Irina Bagyan (bitop AG, Witten, Germany). 2-Oxoglutarate (disodium salt) was purchased from Sigma. Anhydrotetracycline hydrochloride, desthiobiotin, and Strep-Tactin Superflow chromatography material were obtained from IBA GmbH (Göttingen, Germany).

Bacterial Strains, Media, and Growth—The *Escherichia coli* strain DH5α (Invitrogen) was used for the propagation of the *ectD*$^+$ plasmid pMP40 (22, 46). It was grown at 37 °C in Luria-Bertani (LB) liquid medium or on LB agar plates containing ampicillin (100 μg ml^{-1}) to select for the presence of the plasmid. Heterologous overproduction of the *S. alaskensis* EctD protein was carried out in the *E. coli* B strain BL21 (pMP40) in minimal medium A (47) containing 0.5% (w/v) glucose as carbon source, 0.5% (w/v) casamino acids, 1 mM $MgSO_4$, and 3 mM thiamine.

Site-directed Mutagenesis of the Sa-ectD Gene—To assess the contribution of amino acids predicted by structural analysis to be involved in the binding of the 5-hydroxyectoine molecule, or predicted to contribute to interactions between the *Sa*EctD monomers, we performed site-directed mutagenesis. For these experiments, we used the QuikChange Lightning mutagenesis kit (Stratagene, La Jolla, CA) and custom-synthesized mutagenic DNA primers; the DNA primers had a typical length of 25 nucleotides and were purchased from Biomers (Ulm, Germany). To ensure the presence of the desired mutation(s) and the absence of unwanted alterations within the mutagenized *ectD* gene, the DNA sequence of the entire coding region was determined (Eurofins MWG GmbH, Ebersberg, Germany) for each *ectD* mutant allele. DNA of plasmid pMP40 carrying the *Sa-ectD* wild-type gene was used as the template for the site-directed mutagenesis experiments. The following *Sa-ectD* gene variants were isolated: pWN20 (Gln-127 to Ala (CAG to GCG)), pWN21 (Arg-139 to Ala (AGG to GCG)), pWN22 (Glu-140 to Ala (GAG to GCG)), pWN23 (Thr-149 to Ala (ACC to

GCC)), pWN24 (Trp-150 to Ala (TGG to GCG)), pWN25 (Arg-280 to Ala (CGC to GCC)), and the double mutant pWN26 (Arg-139 to Ala (AGG to GCG) and Glu-140 to Ala (GAG to GCG)). These *Sa*EctD variants were overproduced in the *E. coli* B strain BL21 and purified by affinity chromatography. They were functionally assessed by the previously described ectoine hydroxylase enzyme assay (22, 46).

Overproduction and Purification of the Recombinant EctD Protein—Plasmid pMP40 is a derivative of the expression vector pASK-IBA3 (IBA, Göttingen, Germany) in which the transcription of the *ectD* gene (accession number YP_617990) from *S. alaskensis* (45) is positioned under the control of the TetR-responsive and anhydrotetracycline hydrochloride-inducible *tet* promoter carried by the backbone of the pASK-IBA3 expression vector (43, 46). In this plasmid, a nine-amino acid *Strep*-tag-II affinity peptide encoded by a short synthetic DNA sequence is fused to the 3′ end of the *ectD*-coding region to allow the purification of the encoded *Sa*EctD-*Strep*-tag-II protein by affinity chromatography using Strep-Tactin Superflow material. Overproduction and purification of this recombinant protein for crystallization experiments was carried out as described (46). 200–300 mg of *Sa*EctD-*Strep*-tag-II protein/liter of culture was routinely obtained, and the protein was concentrated with Vivaspin 6 columns (Sartorius Stedim Biotech GmbH, Göttingen, Germany) to about 10 mg ml^{-1} (in 20 mM TES buffer, pH 7.5, 80 mM NaCl) before it was used for crystallization trials. The purity of the obtained *Sa*EctD-*Strep*-tag-II protein preparations was assessed on 12% SDS-polyacrylamide gels, and their iron content was determined with the aid of a colorimetric assay (27, 48).

Ectoine Hydroxylase Enzyme Activity Assay—Ectoine hydroxylase enzyme activity of the *Sa*EctD-*Strep*-tag-II protein was determined under previously described buffer and assay conditions (26, 27, 46). Specifically, we monitored the EctD-mediated conversion of ectoine into 5-hydroxyectoine in a 30-μl reaction volume that contained 6 mM ectoine, 10 mM 2-oxoglutarate, 1 mM $FeSO_4$, 20 mM TES, pH 8.0, and 100 mM KCl. 15 μg of either the EctD wild-type protein or the particular *Sa*EctD mutant protein under study was added to the reaction mixture. Each assay was run for 10 min at 40 °C under vigorous aeration. The enzyme reaction was stopped by adding 30 μl of acetonitrile (100%) to the reaction vessel. The substrate ectoine and the reaction product 5-hydroxyectoine were analytically separated from each other on a GROM-SIL Amino-1PR column (125 × 4 mm with a particle size of 3 μm); it was purchased from GROM (Rottenburg-Hailfingen, Germany). The conversion of ectoine to 5-hydroxyectoine by the purified *Sa*EctD-*Strep*-tag-II protein was monitored with a UV-visible detector integrated into a FPLC system (SYKAM, Fürstenfeldbruck, Germany) by measuring the absorbance of these solutes at a wavelength of 210 nm (22, 24, 27). The amount of ectoine remaining in the enzyme assay and the amount of 5-hydroxyectoine formed by the wild-type and mutant EctD proteins were quantified using the ChromStar 7.0 software package (SYKAM, Fürstenfeldbruck, Germany). The data shown for each mutant were derived from two independent *Sa*EctD preparations, and each *Sa*EctD protein solution was assayed three times for its enzyme activity.

Determination of the Oligomeric State of Purified SaEctD and Mutant Derivatives by Conventional Size-exclusion Chromatography and HPLC-MALS—To determine the oligomeric state of the *Sa*EctD-*Strep*-tag-II protein in solution, we used conventional size-exclusion chromatography and high performance liquid chromatography coupled to multiangle light scattering detection (HPLC-MALS). Size-exclusion chromatography was performed with a HiLoad 16/600 Superdex 200pg column (GE Healthcare) equilibrated and run in a 20 mM TES buffer, pH 7.5, containing 150 mM NaCl under conditions described previously (22). The size-exclusion column was standardized with a gel filtration markers kit (Sigma). For HPLC-MALS analysis, a Bio SEC-5 HPLC column (Agilent Technologies Deutschland GmbH, Böblingen, Germany) with a pore size of 300 Å was equilibrated with 20 mM TES, pH 7.5, 80 mM NaCl for HPLC using a system from Agilent Technologies connected to a triple-angle light-scattering detector (miniDAWN TREOS, Wyatt Technology Europe GmbH, Dernbach, Germany) followed by a differential refractive index detector (OPTILab T-rEX, Wyatt Technology). Typically, 100 μl of purified *Sa*EctD (2.0 mg ml^{-1}) was loaded onto the Bio SEC-5 HPLC column, and the obtained data were analyzed with the ASTRA software package (Wyatt Technology).

Crystallization of the SaEctD Protein—For apo-*Sa*EctD, the crystallization trials were performed using the sitting-drop vapor diffusion method at 20 °C. 1.5 μl of the homogeneous protein solution of *Sa*EctD-*Strep*-tag-II (10 mg ml^{-1} in 20 mM TES, pH 7.5, 80 mM NaCl) was mixed with 1.5 μl reservoir solution containing 100 mM MES, pH 6.0, 200 mM calcium acetate, 30% (w/v) PEG 400, and 1.5 mM *n*-dodecyl-*N,N*-dimethylglycine and equilibrated over th 300 μl reservoir solution. Crystals grew within 6–12 days to their final size of around 30 × 30 × 50 μm^3. For Fe-*Sa*EctD-*Strep*-tag-II in complex with Fe^{2+}, the *Sa*EctD-*Strep*-tag-II enzyme in complex with its iron catalyst was crystallized as described above for apo-*Sa*EctD-*Strep*-tag-II protein except that the protein solution was premixed with 100 mM $Fe(II)Cl_2$ to a final concentration of 4 mM and incubated on ice for 10–15 min. In addition, the solution contained 3.5 mM *n*-dodecyl-*N,N*-dimethylglycine. Crystals grew within 6–12 days at 20 °C to their final size of around 40 × 40 × 180 μm^3. For Fe-*Sa*EctD-*Strep*-tag-II in complex with 2-oxoglutarate and 5-hydroxyectoine, the *Sa*EctD-*Strep*-tag-II protein was mixed with $Fe(II)Cl_2$ as described above, and 2-oxoglutarate was subsequently added to the protein solution to a final concentration of 40 mM. After 30 min of incubation on ice, 5-hydroxyectoine was added to the solution to a final concentration of 40 mM. This mixture was then incubated for 1 h on ice before crystallization trials were conducted. *Sa*EctD crystals were grown by mixing 1.5 μl of protein solution with 1.5 μl of reservoir containing 100 mM MES, pH 6.0, 200 mM calcium acetate, 30% (w/v) PEG 400, and 25 mM *n*-octyl-β-D-glycoside; they grew within 6–12 days to their final size of around 40 × 40 × 70 μm^3. All crystals were cryoprotected by carefully adding 1 μl of 100% glycerol to the crystallization drop before the crystals were frozen in liquid nitrogen.

Data Processing and Structure Determination—Data sets were collected from a single crystal obtained from the various crystallization trials (apo-*Sa*EctD, Fe-*Sa*EctD, and Fe-*Sa*EctD/

2-oxoglutarate/5-hydroxyectoine) at the ERSF beamline ID23eh2 (Grenoble, France) at 100 K. These data sets were processed using the XDS package (49) and scaled with XSCALE (50). Initial phases were obtained by molecular replacement using the program PHASER (51) with the crystal structure of the *V. salexigens* EctD protein (PDB code 3EMR) as the template (44). Model building and refinement were performed using COOT (52) and REFMAC5 (53). Data refinement statistics and model content are summarized in Table 1. The structures were deposited at the Protein Data Bank (Brookhaven, NY) under the following accession codes: 4MHR for the apo-*Sa*EctD protein, 4MHU for the Fe-*Sa*EctD protein, and 4Q5O for Fe-*Sa*EctD/2-oxoglutarate/5-hydroxyectoine crystal structure.

Database Searches for EctD-related Proteins—We used the amino acid sequence (accession number YP_617990) from *S. alaskensis* (45) to search microbial genomes for EctD-related proteins in the databases of the National Center for Biotechnology Information (NCBI) (www.ncbi.nlm.nih.gov) and of the United States Department of Energy Joint Genomic Institute) (jgi.doe.gov). Amino acid sequences of EctD-type proteins were aligned as described previously (22, 43).

Figure Preparation of Crystal Structures—Figures of the crystal structure of the *Sa*EctD protein were prepared using the PyMOL software package and Chimera.

RESULTS

Biochemical Properties of the Ectoine Hydroxylase from S. alaskensis and its Oligomeric State in Solution—The ectoine hydroxylase studied here originates from *S. alaskensis*, a microorganism that is well adapted to a life in chilly ocean water systems (45). Despite this permanently cold habitat of the producer microorganism, the *Sa*EctD enzyme itself is thermostable (22). The kinetic properties of the *Sa*EctD protein (with K_m values of 9.8 ± 0.5 and 2.7 ± 0.3 mM for the substrate ectoine and the co-substrate 2-oxoglutarate, respectively, and a catalytic efficiency (k_{cat}/K_m) of 0.12 mM^{-1} s^{-1}) resemble those of other biochemically studied ectoine hydroxylases (22, 26, 27).

We used for our studies a recombinant *Sa*EctD-*Strep*-tag-II protein that carries a nine-amino acid tag at its carboxy terminus to allow affinity purification on Strep-Tactin Superflow material (22, 46). To determine the oligomeric state and to validate the monodispersity of the EctD protein in solution, we carried out a HPLC-MALS analysis. The normalized elution profiles from the UV, refractive index, and light scattering detectors revealed one symmetric peak indicating that the protein solution was homogeneous and monodisperse. After determining protein concentration by the refractive index, a molecular mass of 70.73 ± 1.1 kDa was obtained for the *Sa*EctD-*Strep*-tag-II protein (Fig. 2). This molecular mass corresponds very well to the theoretical molecular mass of a dimer of the recombinant protein (calculated molecular mass of the monomer, including the *Strep*-tag-II affinity peptide: 35.29 kDa) (46). We therefore conclude that the ectoine hydroxylase from *S. alaskensis* is a dimer in solution, a conclusion that is in agreement with the suggested quaternary structures of six other EctD proteins that have been assessed by conventional size exclusion chromatography (22).

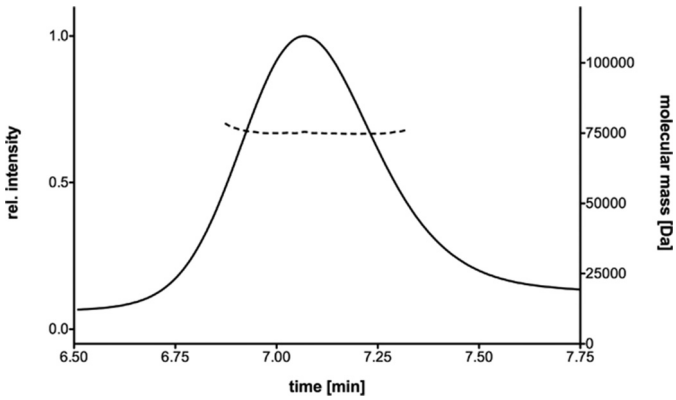

FIGURE 2. **Determination of the oligomeric state of the purified *Sa*EctD-*Strep*-tag-II protein by HPLC-MALS analysis.** *Black line,* normalized refractive index detector signal; *black dotted line,* calculated protein mass.

Crystallization of the SaEctD-Strep-tag-II Protein—By slightly varying the previously used overproduction conditions for the *Sa*EctD-*Strep*-tag-II protein in *E. coli* (22), we were able to increase the amounts of the recovered *Sa*EctD-*Strep*-tag-II protein/liter of culture about 10-fold to 200–300 mg (46). However, although the modified overproduction procedure aided the provision of large amounts of protein for crystallization trials, this also reduced the iron content (44) of the *Sa*EctD-*Strep*-tag-II protein preparation to about 0.13 mol of iron/mol of protein and thereby caused a strong decrease in ectoine hydroxylase activity. By adding $FeSO_4$ or $FeCl_2$ to the purified protein solution, the ectoine hydroxylase activity could be restored, and this allowed us to obtain crystals of the *Sa*EctD-*Strep*-tag-II protein in its apo- and iron-bound forms. The crystals of the apo-*Sa*EctD and Fe-*Sa*EctD proteins diffracted to a resolution of 2.1 and 2.64 Å, respectively.

Co-crystallization experiments of *Sa*EctD with its substrate ectoine were not successful, despite that a large number of well diffracting crystals were obtained; however, none of these contained the ectoine ligand as revealed by x-ray analysis. The co-crystallization of a protein with its enzymatic reaction product has been successfully used to obtain informative crystal structures (54). When applied to the *Sa*EctD protein, it yielded crystals with good diffraction properties, but none of them showed any electron density for 5-hydroxyectoine. We then turned to an approach in which we added iron, 2-oxoglutarate, and 5-hydroxyectoine in a stepwise manner to the *Sa*EctD-*Strep*-tag-II protein in which we incubated the protein solution containing a high concentration of the ligands for at least 1.5 h on ice before it was used for crystallization trials. In this way, we obtained crystals that diffracted to a resolution of 2.56 Å and that contained the iron ligand, the co-substrate 2-oxoglutarate, and the EctD-enzyme reaction product 5-hydroxyectoine.

All three crystal structures of the *Sa*EctD protein were solved by molecular replacement using the crystal structure of the *V. salexigens* (*Vs*EctD) ectoine hydroxylase (PDB code 3EMR) (44) as the search model. A summary of the data collection statistics, refinement details, and model content is given in Table 1.

Overall Fold of the SaEctD Protein—The amino acid sequences of the *Vs*EctD and *Sa*EctD possess an amino acid

TABLE 1
Data collection and refinement statistics for the apo- and iron-bound forms of the ectoine hydroxylase and of the iron-, 2-oxoglutarate-, and 5-hydroxyectoine-bound forms of the *Sa*EctD protein

	Apo-*Sa*EctD	Fe-*Sa*EctD	Fe-*Sa*EctD/2-oxoglutarate/5-hydroxyectoine
Crystal parameters at 100 K			
Space group	C222	$P2_12_12_1$	$P2_12_12_1$
Unit cell parameters			
a, b, c (Å)	83.48, 86.51, 95.34	78.16, 87.52, 96.05	81.00, 87.08, 94.88
$\alpha = \beta = \gamma$ (°)	90	90	90
Data collection and processing			
Wavelength (Å)	0.87260	0.87260	0.87260
Resolution (Å)	30-2.1 (2.2-2.1)	30-2.64 (2.8-2.64)	30-2.56 (2.8–2.56)
Mean redundancy	4.2 (4.1)	4.9 (5.0)	3.9 (3.8)
Unique reflections	20,251	18,652	18,360
Completeness (%)	99.7 (99.8)	99.6 (99.9)	99.8 (99.8)
I/σ	15.1 (2.8)	19.8 (2.9)	14.8 (1.8)
R_{sym} (%)	6.2 (49.9)	5.8 (58.9)	7.3 (56.2)
Refinement statistics			
R_F (%)	16.7	20.6	20.6
R_{free} (%)	21.8	26.7	27.8
r.m.s.d. from ideal			
Bond lengths (Å)	0.019	0.0115	0.009
Bond angles (°)	1.8	1.5	1.3
Average B-factors (Å^2)	43.1	63.8	54.4
Ramachandran plot			
Most favored (%)	96.3	93.4	92.1
Allowed (%)	3	5.1	6.6
Generously allowed (%)	0.7		
Disallowed (%)		1.5	1.4
Model content			
Monomers/ASU	1	2	2
Protein residues	2–192, 210–301	2–192, 210–301	2–192, 210–301
Ligand		2 iron, 1 D9G	2 iron, 2 AKG, 2 6CS
Water molecules	108		

sequence identity of 51% (for an alignment see Fig. 3). An overall comparison of the three newly determined *Sa*EctD crystal structures with that of the previously determined structure of *Vs*EctD revealed a high degree of identity with an r.m.s.d. that ranges from 1.3 to 1.6 Å over 279 C-α atoms. An even lower r.m.s.d. of 0.5– 0.8 Å was found when the three different *Sa*EctD structures were compared with each other. Hence, neither the binding of the catalytically critical iron ligand nor of the substrate 2-oxoglutarate and 5-hydroxyectoine triggered a strong change in the overall conformation of the EctD protein.

Because the monomers of all three *Sa*EctD structures are nearly identical in overall shape, we describe in the following section only the overall fold for the apo-*Sa*EctD protein. The *Sa*EctD crystal structure consists of a double-stranded β-helix core surrounded and stabilized by a number of α-helices (Fig. 4*A*). This core, also known as the jelly roll or cupin fold (38, 39), is formed by two four-stranded anti-parallel β-sheets that are arranged in the form of a β-sandwich (Fig. 4*A*). This type of architecture has previously been observed not only for the *Vs*EctD protein (22, 44) but also for many other non-heme-containing iron(II) and 2-oxoglutarate-dependent dioxygenases (38–40). Examples are the EctD-related structures of the human phytanoyl-CoA hydroxylases PhyH (PDB code 2A1X; r.m.s.d. of 2.6 Å over 252 C-α atoms when compared with the *Sa*EctD structure) (55) and PhyHD1A (PDB code 2OPW r.m.s.d. of 2.2 Å over 286 C-α atoms) (56) and the halogenases SyrB2 from *Pseudomonas syringae* (PDB code 2FCV; r.m.s.d. of 2.9 Å over 299 C-α atoms) (57), CytC3 from a *Streptomyces* soil isolate (PDB code 3GJA; r.m.s.d. of 3.0 Å over 204 C-α atoms) (58), and CurA from the cyanobacterium *Lyngbya majuscula* (PDB code 3NNM; r.m.s.d. of 3.3 Å over 222 C-α atoms) (59). This structural comparison shows that the core of the EctD protein, its cupin-type fold, is very similar to these proteins; however, the rest of EctD differs from the structurally compared proteins and thereby yields higher r.m.s.d. values.

In each of the three *Sa*EctD crystal structures, a large loop (amino acids 191–210) is disordered and hence not visible in the electron density map; the corresponding region was therefore not included in the *Sa*EctD models. By amino acid sequence alignment (Fig. 3), this loop corresponds to residues 195–211 in the *Vs*EctD ectoine hydroxylase, and it is also disordered in both crystal structures of this protein (22, 44). Notably, in the ligand-free crystal structures of the phytanoyl-CoA hydroxylases PhyH (55), the asparagine hydroxylase AsnO from *S. coelicolor* (60), the L-arginine oxygenase VioC from *Streptomyces vinaceus* (61), and the taurine dioxygenases from *E. coli* and *Pseudomonas putida* (62), a similar loop is disordered as well and became only visible in crystal structures with bound substrates. It is thought that this mobile loop functions as a lid that shields the enzyme reaction chamber during catalysis from the solvent.

Dimer Interface of the SaEctD Protein—The three crystal structures of the ectoine hydroxylase from *S. alaskensis* displayed a different crystal packing (as observed by the different symmetry of the crystals) and protein composition in the asymmetric unit (ASU) of the crystals. In apo-*Sa*EctD, the asymmetric unit contains a monomer, whereas the ASUs of Fe-*Sa*EctD and Fe-*Sa*EctD/2-oxoglutarate/5-hydroxyectoine both include dimers. The monomers in the latter dimer are however differently oriented (Fig. 5). Because the *Sa*EctD protein is a dimer in solution (see above and Fig. 2), we inspected the crystal packing and analyzed the monomer/monomer interactions to elucidate

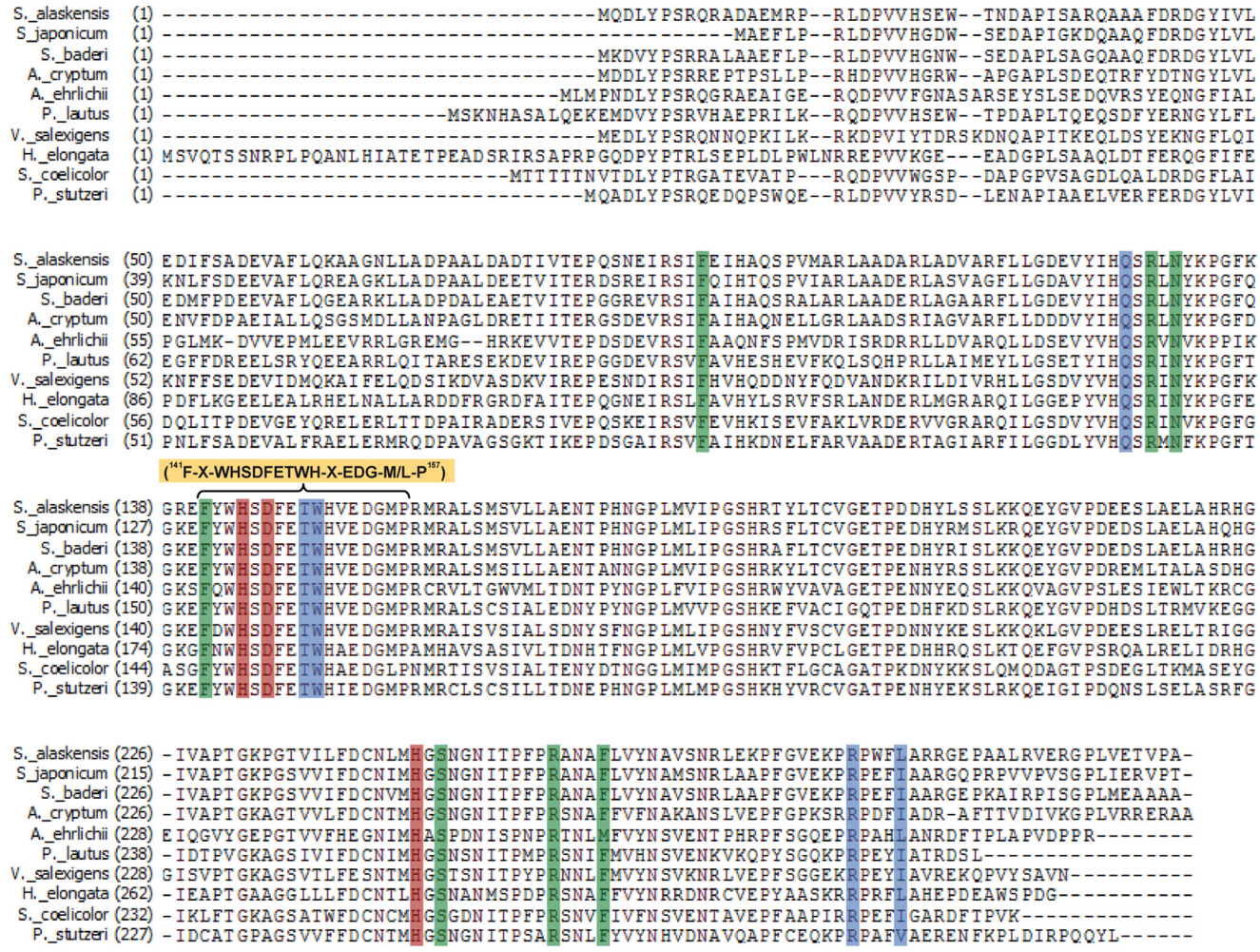

FIGURE 3. **Alignment of the amino acid sequences of 10 EctD-type proteins.** The *S. alaskensis* ectoine hydroxylase was used as the search query, and the EctD-type proteins from *Sphingobium japonicum* (WP_006964700) and *Sphingobium baderi* (WP_021243884) were found as the most closely related proteins to the *Sa*EctD (YP_617990) enzyme. The EctD enzymes from *Acidiphilium cryptum* (AER00258), *Alkalilimnicola ehrlichii* (AER00257), *Paenibacillus lautus* (ACX67869), *Virgibacillus salexigens* (AAY29689), *Halomonas elongata* (YP_003899077), *S. coelicolor* (Q93RV9), and *Pseudomonas stutzeri* (WP_011911424) have been functionally characterized and are *bona fide* ectoine hydroxylases. Residues involved in the binding of the iron catalyst are marked in *red*; those that mediate the binding of the 2-oxoglutarate co-substrate are labeled in *green*, and residues contacting the 5-hydroxyectoine molecule are marked in *blue*. Residues His-144 and Asp-146 of the *Sa*EctD protein are involved both in the binding of the iron catalyst and also of the 5-hydroxyectoine molecule. The string of the 17 amino acids that serves as the consensus sequence of ectoine hydroxylases is labeled in *yellow*.

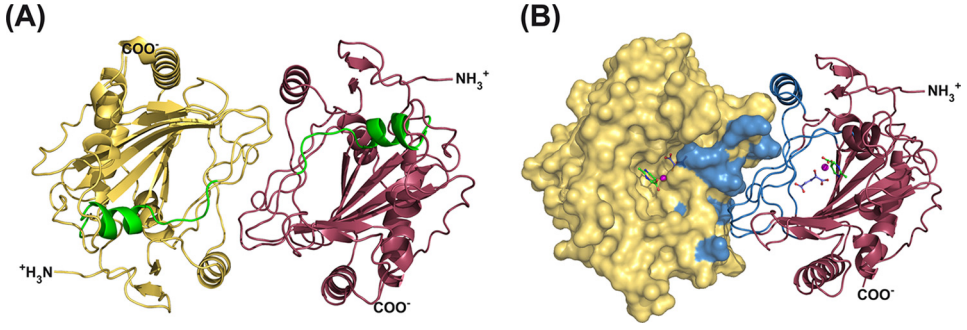

FIGURE 4. **Dimer structure of the *Sa*EctD-*Strep*-tag-II protein in complex with iron, 2-oxoglutarate, and 5-hydroxyectoine.** *A, ribbon* representation of the crystal structure of the *Sa*EctD-*Strep*-tag-II protein in complex with iron, 2-oxoglutarate, and 5-hydroxyectoine (PDB code 4Q5O); the ligands have been omitted for simplicity. The two monomers are differently colored, and the region corresponding to the EctD signature sequence motif is highlighted in *green*, and the N and C termini of the protein are indicated. *B*, representation of the monomer/monomer interface of the *Sa*EctD-*Strep*-tag-II dimer in complex with all three substrates. One of the monomers is shown in surface representation, and the second monomer is represented in a *ribbon* format. Residues and regions that interact in the dimer are highlighted in *blue*. The iron catalyst is represented as a *sphere* (in *magenta*) and the co-substrate 2-oxoglutarate and the EctD enzyme reaction product, 5-hydroxyectoine, are shown in *ball and stick* representation.

which dimer in the crystals might represent the physiologically relevant dimer (Fig. 5). The monomers in the ASUs of apo-*Sa*EctD form also a dimer assembly through crystal symmetry, similar to that found in the *Sa*EctD/2-oxoglutarate/5-hydroxyectoine crystal structure. The monomers in the Fe-*Sa*EctD dimer are slightly shifted toward each other when

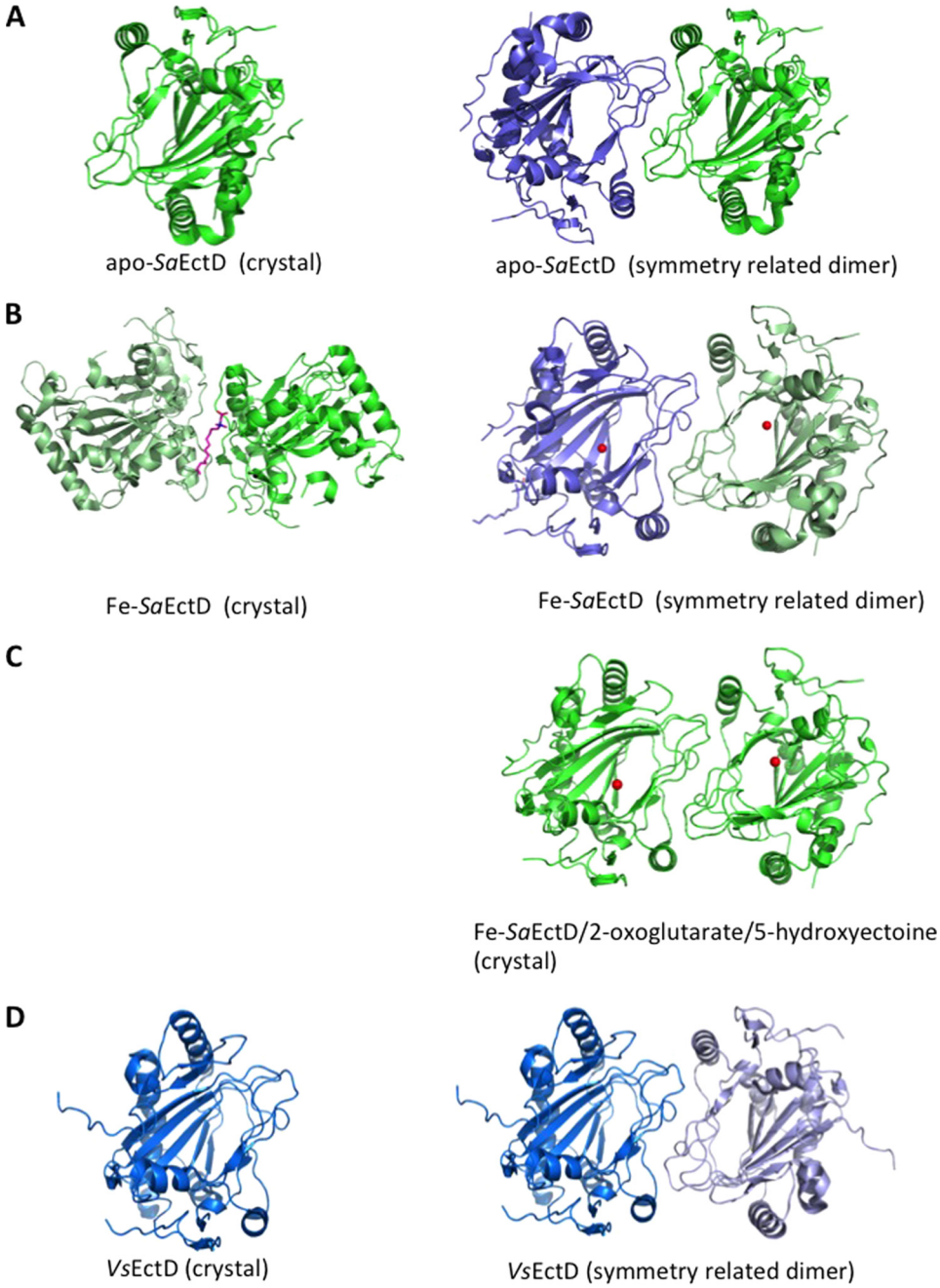

FIGURE 5. **Dimer assemblies of the *Sa*EctD protein.** Shown are the compositions of the ASUs of the apo-*Sa*EctD, Fe-*Sa*EctD, and Fe-*Sa*EctD/2-oxoglutarate/5-hydroxyectoine crystals, and the associated dimer of the *Sa*EctD protein obtained by symmetry-related molecules. *A,* apo-*Sa*EctD was crystallized containing a monomer in the ASU (highlighted in *green*). The corresponding dimer was obtained by highlighting the symmetry-related molecules. The second monomer of the dimer is shown in *blue. B,* Fe-*Sa*EctD contained a dimer in the ASU (the single monomers are shown in *light* and *dark green*) and an extra *n*-dodecyl-*N,N*-dimethylglycine (highlighted in *red*) captured from the crystallization solution; it was bound between the two monomers. The dimer found by symmetry-related molecules is highlighted in *green* and *blue* in the *right panel*. The iron molecules are shown as *red spheres*. *C,* Fe-*Sa*EctD/2-oxoglutarate/5-hydroxyectoine crystals contained a dimer in the ASU similar to the other symmetry related dimers. The iron molecules were highlighted as *red spheres*. For clarity we omitted the 2-oxoglutarate and 5-hydroxyectoine from the figure. *D,* crystal structure of the *Sa*EctD-related *V. salexigens* EctD protein (PDB code 3EMR) (44) revealed a monomer in the ASU shown in *blue*. The iron molecules are highlighted in *red*. The symmetry related dimer is shown in the *right panel*.

one compares them to the *Sa*EctD/2-oxoglutarate/5-hydroxyectoine dimer. However, this difference in the Fe-*Sa*EctD structure is likely due to the extra *n*-dodecyl-*N,N*-dimethylglycine molecule that was present in the crystallization solution and that is bound in between the two monomers. This leads to a different crystal packing in the ASU. In contrast, when looking at the Fe-*Sa*EctD dimer composed of the symmetry-related monomers (Fig. 5*B*, *right panel*), we found the same arrangement in the ASU of the *Sa*EctD/2-oxoglutarate/5-hydroxyectoine crystal (Fig. 5*C*). The only other member of the EctD superfamily that has been so far crystallized is the *Vs*EctD protein in forms that either possess or lack the iron catalyst (22, 44). In these structures, the ASU contains a monomer, although gel filtration analysis showed that the *Vs*EctD protein is a dimer in solution (22). We re-analyzed the crystal packing of the *Vs*EctD protein and found a similar dimer as observed in the *Sa*EctD/

2-oxoglutarate/5-hydroxyectoine crystal structure presented here (Fig. 5*D*).

To ensure that the dimer observed in the *Sa*EctD/2-oxoglutarate/5-hydroxyectoine crystal structure is also a dimer in solution, we studied its quaternary composition under the very same buffer and substrate conditions that were used in the co-crystallization experiments by analyzing these samples using size-exclusion chromatography-MALS. The molecular mass determined for the *Sa*EctD-*Strep*-tag-II protein by this experiment was 75.02 ± 1.8 kDa, which corresponds to a dimeric state of the protein (calculated theoretical mass of the iron, 2-oxoglutarate, and 5-hydroxyectoine bound dimer, 71.3 kDa). We then analyzed the dimer interface using the PDBePISA software (63). We found 10 potential monomer/monomer interaction regions (Table 2) and observed that the involved amino acids are all located in loop areas pointing from one monomer to the other monomer (Fig. 4*B*). However, inspection of the aforementioned loop regions implicated in forming the dimer interface revealed that their amino acid sequences are only moderately conserved, as judged by consulting a previous alignment of 433 EctD-type proteins (22, 43).

Residues Arg-139 and Glu-140 seemed to make most contributions to dimer formation (Table 2). To investigate their potential role for the quaternary structure and their possible corresponding influence on enzyme activity, we targeted these residues of *Sa*EctD by site-directed mutagenesis. We replaced them individually by Ala residues and also constructed the respective double mutant. Each of these three EctD variants was fully catalytically active (Table 3). Contrary to expectations, each of these EctD proteins still formed dimers in solution, as assessed by conventional size-exclusion chromatography This is documented for the double mutant EctD protein (Arg-139/Ala and Glu-140/Ala) in Fig. 6.

TABLE 2

Monomer/monomer interactions in the *Sa*EctD protein in complex with Fe-2-oxoglutarate and 5-hydroxyectoine

The amino acids involved in the dimer interface are listed, and the distance and type of interaction ((H), hydrogen bond; (S), salt bridge) are indicated.

Monomer A	Monomer B	Distance (type)
Glu-140 (OE1)	Arg-139 (NH_2)	2.6 Å (H)
Glu-140 (OE1)	Arg-139 (NE)	3.7 Å (S)
Glu-140 (OE1	Arg-139 (NH1)	3.7 Å (S)
Glu-140 (OE1)	Arg-139 (NH_2)	2.5 Å (S)
His-174 (NE2)	Ile-226 (O)	3.3 Å (H)
Glu-214 (OE2)	Lys-137 (NZ)	3.6 Å (S)
Gly-249 (O)	Asn-248 (ND2)	3.3 Å (H)
Ile-251 (O)	Trp-143 (NE1)	3.1 Å (H)

TABLE 3

Conversion of ectoine into 5-hydroxyectoine by *Sa*EctD mutants

The conversion of ectoine into 5-hydroxyectoine by the *Sa*EctD protein was monitored in a reaction that contained 6 mM ectoine as the substrate, 10 mM 2-oxoglutarate as the co-substrate, and 15 μg of the EctD protein under study. The amount of 5-hydroxyectoine was measured after 10 min.

EctD variant	5-Hydroxyectoine	Proposed role in
	mM	
Wild type	4.93 ± 0.26	
Q127A	0.04 ± 0.03	Ectoine binding
T149A	0.17 ± 0.05	Ectoine binding
W150A	0.09 ± 0.06	Ectoine binding
R280A	0.31 ± 0.14	Ectoine binding
R139A	5.01 ± 0.15	Dimerization
E140A	4.93 ± 0.20	Dimerization
R139A/E140A	4.72 ± 0.31	Dimerization

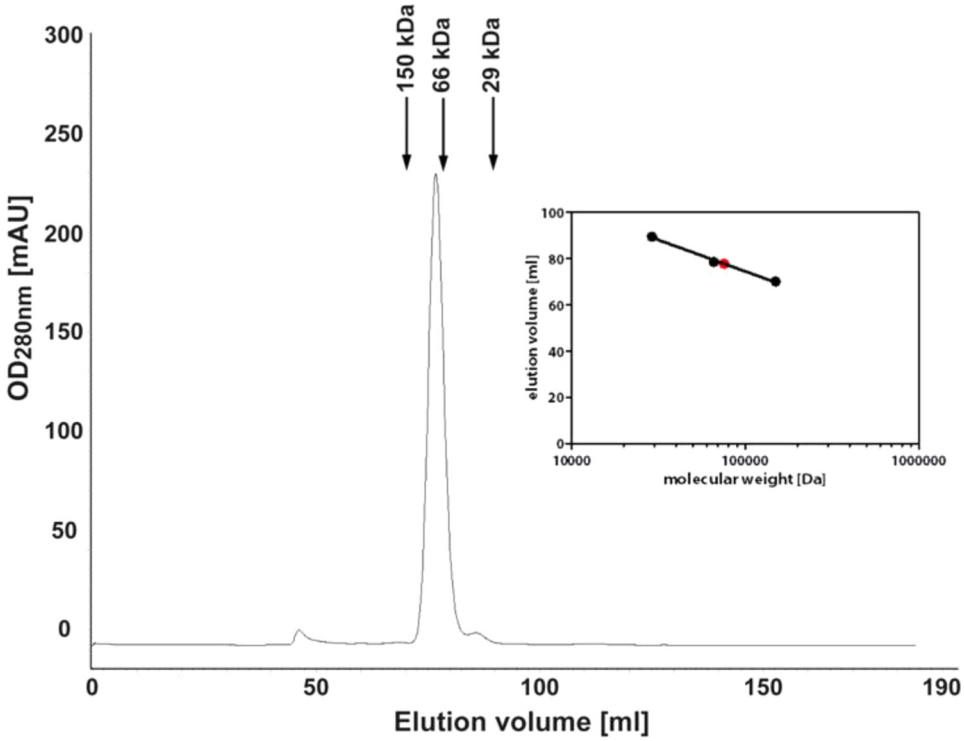

FIGURE 6. **Size-exclusion chromatography of the *Sa*EctD double mutant (R139A/Q140A).** The purified mutant protein (5 μg) was loaded onto a HiLoad 16/600 Superdex 200pg column (GE Healthcare) equilibrated and run in a 20 mM TES buffer, pH 7.5, containing 150 mM NaCl. The column run was performed at 15 °C. The size-exclusion column was standardized with a gel filtration markers kit (Sigma). The elution profile of the mutant EctD protein is shown, and *arrows* indicate that of relevant marker proteins. The *inset* shows a plot of the molecular mass (given in Da) of marker proteins (*black dots*) and of the EctD (R139A/Q140A) variant (*red dot*) *versus* the elution volume (given in ml).

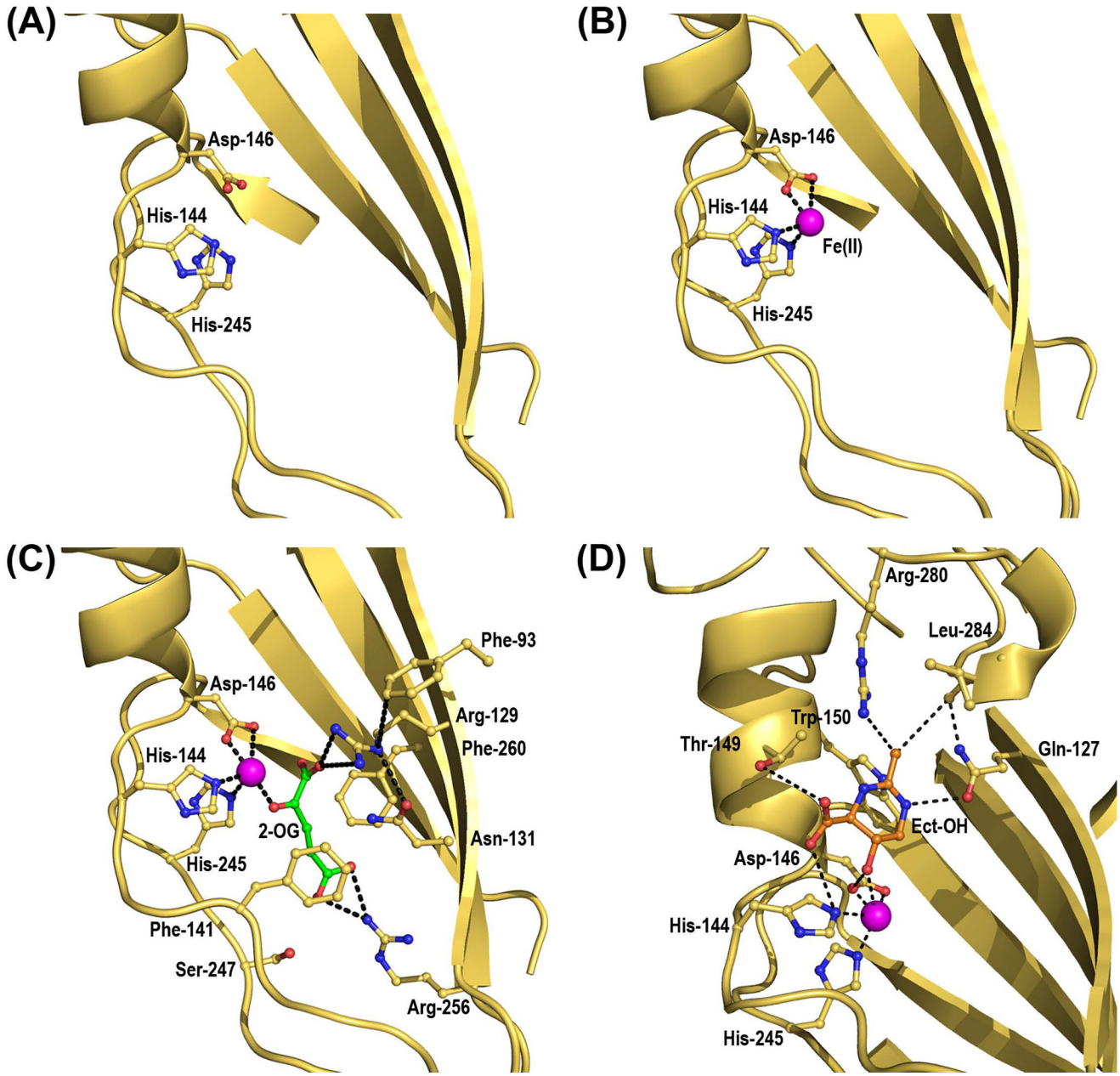

FIGURE 7. **Crystal structures of the *Sa*EctD-*Strep*-tag-II protein in its apo- and iron-bound forms and in complex with iron, 2-oxoglutarate, and 5-hydroxyectoine.** *Ribbon* representation of the catalytic core of the iron-free (PDB code 4HMR) (*A*) and iron-bound (PDB code 4MHU) (*B*) forms of the *S. alaskensis* ectoine hydroxylase. The ribbon representations of the catalytic core of the ectoine hydroxylase shown in *C* and *D* are both based on a crystal structure that contained the iron catalyst, the 2-oxoglutarate co-substrate, and the product of the EctD-catalyzed enzyme reaction, 5-hydroxyectoine (PDB code 4Q5O). In the structure shown in *C*, only the binding of the iron catalyst and the 2-oxoglutarate (*2-OG*) molecules are shown, and the structure shown in *D* highlights only the binding of the iron catalyst and the captured 5-hydroxyectoine (*Ect-OH*) molecule. Amino acids involved in ligand binding are represented as *sticks*.

Architecture of the Iron-binding Site—Because the overproduction conditions perfected for the large scale isolation of the ectoine hydroxylase in *E. coli* (see above) foster the synthesis of iron-free recombinant *Sa*EctD-*Strep*-tag-II protein, we were able to obtain *Sa*EctD crystal structures that either possessed or lacked the iron catalyst (Fig. 7, *A* and *B*). This was accomplished by adding or leaving out $Fe(II)Cl_2$ in the crystallization trials.

The iron ligand is bound in the *Sa*EctD protein via interaction with two histidine side chains, His-144 and His-245, and that of Asp-146 (Fig. 7*B*). These residues form a structurally well conserved H*X*(D/E) . . . H motif, the so-called 2-His-1-carboxylate facial triad, forming a type of mononuclear iron center found in many members of the dioxygenase superfamily (37–40, 64). The three iron-binding residues are fully conserved among a group of 433 aligned EctD-type proteins (22). Two of the iron-coordinating residues (His-144 and Asp-146) in the *Sa*EctD protein are part of a 17-amino acid residue region that is strictly conserved in ectoine hydroxylases (22, 27, 44). This EctD signature sequence spans an extended α-helix and a linked short β-sheet lining one side of the DSBH/cupin fold (Fig. 4*A*). We compared the structural arrangement of this region in the apo- and iron-bound forms of *Sa*EctD (Fig. 7, *A*

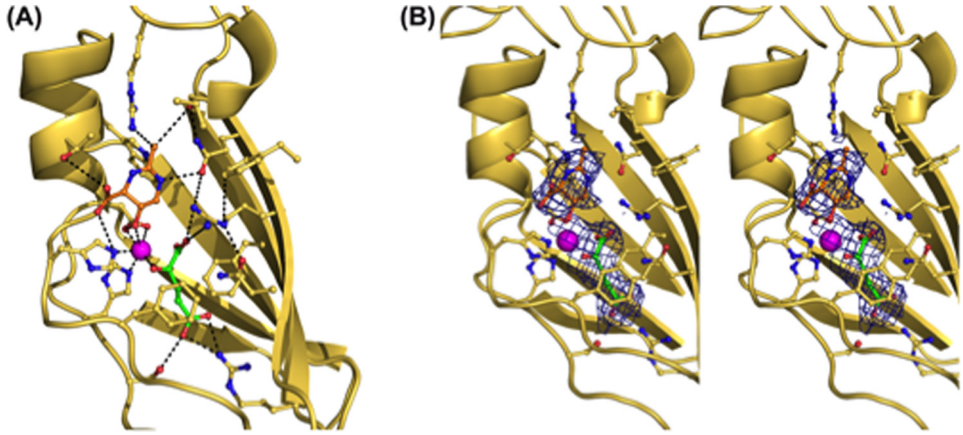

FIGURE 8. **Architecture of the active site of the *S. alaskensis* ectoine hydroxylase.** The crystal structure shown in *A* highlights the network of interactions allowing the binding of the iron catalyst and of the 2-oxoglutarate co-substrate and the EctD-catalyzed enzyme reaction product, 5-hydroxyectoine. Amino acids involved in ligand binding are represented as *sticks*. In (*B*) the electron density of an omit map (calculated by the Phenix software) of the 2-oxoglutarate and 5-hydroxyectoine molecules captured by the active site of *Sa*EctD is shown as stereo figure. The 2Fo-Fc map was contoured at 1.0 sigma. Both figures are based on data deposited in the PDB under accession code 4Q5O.

and *B*) and observed no significant differences between these two structures, thus reinforcing our conclusion (22) that the capturing of the iron ligand does not induce significant structural changes in the ectoine hydroxylase.

Architecture of the 2-Oxoglutarate-binding Site—In the crystals that we obtained by adding $Fe(II)Cl_2$, the co-substrate 2-oxoglutarate, and the reaction product 5-hydroxyectoine, the densities for the 2-oxoglutarate and 5-hydroxyectoine ligands were clearly visible. We first describe the coordination of the 2-oxoglutarate co-substrate and subsequently that of 5-hydroxyectoine by the EctD protein.

The 2-oxoacid group of 2-oxoglutarate is placed in close vicinity to the iron catalyst in the active site (Fig. 7*C*). Interactions with the side chains of Arg-256, Ser-247, and Phe-141 are key for 2-oxoglutarate binding (Fig. 7*C*). Furthermore, stabilizing interactions of this ligand are formed with the side chain of Arg-129. The precise configuration of the Arg-129 side chain is in turn stabilized through interactions with the side chains of Phe-93 and Asn-131 (Fig. 7*C*). Arg-129 and Asn-131 are part of the DSBH core; however, Phe-93 is positioned in a β-sheet flanking this fold. The Arg-129/Phe-93 and Arg-129/Asn-131 interactions thereby stabilize the conformation of the *Sa*EctD protein as a whole. Loss of these interactions would probably lay the active site of *Sa*EctD more open, possibly rendering it unable to bind any of its substrates in a coordinated fashion. The 2-oxoglutarate ligand within the active site is further stabilized by Phe-260, although this interaction appears to be not very strong because the distance between 2-oxoglutarate and the Phe side chain is almost 4 Å (Fig. 7*C*).

The architecture of the 2-oxoglutarate-binding site of the *Sa*EctD protein is similar to that found in crystal structures of many non-heme containing iron(II) and 2-oxoglutarate-dependent dioxygenases (38–40). It also corresponds closely to that suggested by structural comparison and modeling studies of the ligand-free *Vs*EctD protein (43, 44).

Architecture of the 5-Hydroxyectoine-binding Site—The 5-hydroxyectoine molecule is bound within the active site of *Sa*EctD slightly above the three residues (His-144, His-245, and Asp-146) forming the 2-His-1-carboxylate facial triad and in such a way that the hydroxy group at C5 in the pyrimidine ring points toward the iron catalyst (Fig. 7*D*). It is also positioned in close vicinity to the 2-oxoglutarate co-substrate (Fig. 8*A*). Hence, the spatial orientation of the 5-hydroxyectoine molecule is such as one would expect after the EctD enzyme has completed the hydroxylation of its substrate ectoine (27, 33, 43). The electron densities of the iron catalyst, the 2-oxoglutarate co-substrate, and the reaction product 5-hydroxyectoine are reasonably well resolved in the 2.56 Å *Sa*EctD crystal structure (Fig. 8*B*).

Interactions of the EctD protein with the ring structure of 5-hydroxyectoine and its methyl and carboxyl groups position and stabilize this molecule within the active site (Fig. 7*D*). The side chains of Gln-127, Trp-150, and Arg-280 are directly involved in these interactions; a hydrogen bond to the backbone of Leu-284 and a weak interaction with the side chain of Thr-149 (distance of 3.9–4.0 Å) provide additional stability for the binding of the ligand (Fig. 7*D*). Arg-129 interacts with the side chain of Gln-127 and therefore provides further stability (Fig. 5*A*). In addition, Trp-150, a residue that belongs to the ectoine hydroxylase signature sequence (22, 27, 44), makes contact with the pyrimidine ring of 5-hydroxyectoine (Fig. 7*D*). This residue seems to play a special role in ectoine/5-hydroxyectoine binding because its conservative replacement with either Phe or Tyr residues in the *Vs*EctD enzyme yielded catalytically inactive protein variants (43). This finding suggests that the interactions with the second aromatic ring structure of Trp are important for ligand stabilization. The carboxyl group of 5-hydroxyectoine is coordinated through interactions with Thr-149, a residue of the signature sequence motif, and His-144, which is part of the iron-coordinating 2-His-1-Asp facial triad motif (Fig. 7*D*).

Molecular dynamics simulations were recently used to glean information about the possible location of the ectoine substrate within the crystal structure of the *Vs*EctD protein (43). Despite the moderate affinity of this enzyme for its substrate ectoine (K_m = 5.9 ± 0.3 mM) (22), this modeling approach positioned the ectoine molecule to the same ligand-binding pocket that was revealed through the crystallographic analysis of the

*Sa*EctD protein presented in this study (Fig. 7*D*). However, relative to the spatial orientation of the 5-hydroxyectoine ligand found in the experimentally determined *Sa*EctD crystal structure (Figs. 7*D* and 8*A*), the ectoine molecule is flipped by 180° around its vertical axis when compared with its position in the *in silico* generated model, and it is also slightly tilted (43). In the *Sa*EctD crystal structure, the carboxylate of the 5-hydroxyectoine molecule is stabilized via hydrogen bonds (Figs. 7*D* and 8*A*), although such stabilizing interactions are missing in the *Vs*EctD *in silico* model (43). Interactions with the carboxylate of either ectoine or 5-hydroxyectoine are important for high affinity ligand binding by solute receptor proteins operating in conjunction with either ABC or TRAP transport systems for these compounds (65–67). We therefore surmise that the *Sa*EctD crystal structure in complex with 5-hydroxyectoine (Fig. 8*A*) also reflects the configuration and spatial position of the ectoine substrate when it is captured in the active site by the ectoine hydroxylase prior to catalysis.

Structure-guided Mutagenesis of 5-Hydroxyectoine-contacting Residues—The binding of the iron catalyst and the 2-oxoglutarate co-substrate in non-heme-containing dioxygenases is mediated by structurally well conserved motifs (37–40), and these are also present in the *Vs*EctD (22, 44) and *Sa*EctD proteins (Fig. 7, *B* and *C*). The corresponding residues in the *Vs*EctD protein (Fig. 3) have already been targeted by site-directed mutagenesis and inevitably yielded mutant EctD proteins that were either strongly impaired in their enzyme activity or were catalytically inactive (43). In view of the fact that the corresponding iron- and 2-oxoglutarate-coordinating residues (Fig. 4, *B* and *C*) within the EctD enzyme family are practically completely conserved within a group of 433 inspected EctD-type proteins (22, 43), we have not repeated such experiments with the *Sa*EctD protein. Instead, we have focused on those residues that contact the 5-hydroxyectoine molecule within the ligand-binding site of *Sa*EctD (Fig. 7*D*).

Residues Gln-127, Thr-149, Trp-150, and Arg-280 (Fig. 7*D*) were individually substituted by an Ala residue; Leu-284 was not changed because it makes a backbone contact to 5-hydroxyectoine. Likewise, the 5-hydroxyectoine-contacting residues His-144 and Asp-146 were also not targeted by site-directed mutagenesis because their side chains are not only involved in 5-hydroxyectoine binding but are critical for binding of the iron catalyst as well (Fig. 7, *B* and *D*). The individual substitution of Gln-127, Thr-149, Trp-150, and Arg-280 by Ala residues yielded EctD variants that were either strongly impaired in their enzyme function (Thr-149/Ala and Arg-280/Ala), or almost completely catalytically inactive (Gln-127/Ala and Trp-150/Ala) (Table 3). Fully consistent with these results are data from a mutagenesis study of the *Vs*EctD protein in which the two 5-hydroxyectoine-contacting residues corresponding to Gln-127 and Trp-150 in the *Sa*EctD protein (Fig. 3) have been studied; their replacement yielded enzymatically inactive variants of EctD as well (43). Given the combined data from the site-directed mutagenesis studies of the *Sa*EctD (Table 3) and the *Vs*EctD (43) proteins, it is not unexpected that each residue involved in the binding of 5-hydroxyectoine is completely conserved in an alignment of 433 microbial EctD-type proteins (22, 43).

DISCUSSION

Members of the superfamily of non-heme-containing iron(II) and 2-oxoglutarate-dependent dioxygenases share similar overall structures and enzyme mechanisms, but they can catalyze a diverse set of oxidation reactions (37–41). The ectoine hydroxylase (EctD) belongs to this superfamily and mediates the stereo-specific hydroxylation of the compatible solute ectoine to form 5-hydroxyectoine (27, 68), which thereby gains novel stress-protective and function-preserving properties (11–15, 35, 36). The crystal structures of EctD from the extremophilic bacteria *V. salexigens* (44) and *S. alaskensis* (this study) are most closely related to the human hydroxylases PhyH and PHYD1A (55, 56) and to the microbial halogenases SyrB2, CytC3, and CurA (57–59). It is noteworthy that the substrates of the mentioned halogenases are all tethered via a thioester to the phosphopantetheine arms of acyl carrier proteins of polyketide synthases and nonribosomal peptide synthetases that function within assembly lines directing the synthesis of antibiotics and phytotoxins (57–59). In contrast, ectoine hydroxylases use a freely diffusible small molecule as their substrate (22, 26, 27).

Various quaternary conformations are found for enzymes belonging to the non-heme-containing iron(II) and 2-oxoglutarate-dependent dioxygenase superfamily (37–39, 62). Conventional size-exclusion chromatography (22) and HPLC-MALS analysis (Fig. 2) strongly suggest that ectoine hydroxylases obtained from various producer organisms are all dimers in solution. In the homodimer of the *Sa*EctD crystal structure, the two monomers are oriented in a head to tail fashion and interact through loop regions (Fig. 4).

The crystallographic analysis of the *Sa*EctD protein in complex with all its ligands (Fig. 8*A*) revealed that three residues contribute to iron binding, seven are involved in the binding of 2-oxoglutarate, and seven mediate the binding of 5-hydroxyectoine. Of these 15 residues, His-144 and Asp-146 are simultaneously involved in the binding of the iron catalyst and of 5-hydroxyectoine (Fig. 8*A*).

When one views the overall shape and surface structure of the crystallized EctD proteins as a whole, a deep cavity is immediately apparent in each of the monomers (Fig. 4*B*). The iron ligand, the co-substrate 2-oxoglutarate, and the EctD reaction product 5-hydroxyectoine (and by inference also the substrate ectoine) are all located in this cavity (Fig. 4*B*). As expected, all residues that we deem to be of functional importance for ligand binding and catalysis protrude into this cavity of the EctD protein (Figs. 4*B* and 8*A*).

Multiple cation/π interactions between the delocalized positive charges of the ectoine and 5-hydroxyectoine molecules (Fig. 1) and the side chains of aromatic residues of extracellular ectoine/5-hydroxyectoine-specific solute receptor proteins (EhuB, UehA, and TeaA) that operate in conjunction with either ABC or TRAP transport systems (65–67) are key determinants for high affinity binding of these tetrahydropyrimidines. These ligand-binding proteins possess K_d values in the low micromolar range because they need to scavenge ectoines from scarce environmental resources for use either as osmostress protectants or as nutrients (65–67). Ectoine hydroxy-

lases, however, have K_m values in the low millimolar range (between 5 and 10 mM) (22, 26, 27), and this property might be the reason why one typically finds considerable amounts of ectoine in osmotically stressed microbial cells before 5-hydroxyectoine production sets in (26, 27, 69). In contrast to the aforementioned solute receptor proteins for ectoines (65–67), cation/π interactions do not contribute to 5-hydroxyectoine binding (and by inference to the substrate ectoine as well) by the EctD enzyme (Fig. 5*A*). This might contribute to the rather modest affinity of ectoine hydroxylases for their substrate ectoine (22, 26, 27).

Alignments of the amino acid sequences of ectoine hydroxylases have revealed a signature sequence motif of 17 amino acids in length (F*X*WHSDFETWH*X*EDG(M/L)P) (22, 27, 43, 44) that is, with a few minor exceptions, strictly conserved in 433 EctD-type proteins inspected by us (22). This string of amino acids forms an extended α-helix that is connected to a short β-strand; it structures one side of the EctD cupin barrel (Fig. 4*A*). Not only is the signature sequence region structurally important for the overall fold of the EctD protein but the crystallographic data presented here show that it also contains five residues that contribute in multiple ways to the binding of all three ligands of the ectoine hydroxylase. In the *Sa*EctD protein, these residues include the side chains of His-144 and Asp-146 that are involved in iron binding, Phe-141, which is involved in 2-oxoglutarate binding, and the 5-hydroxyectoine (ectoine)-contacting amino acids His-144, Asp-146, Thr-149, and Trp-150 (Fig. 8).

When one views the *Sa*EctD active site as a whole, an intricate network of interactions between the iron catalyst, the co-substrate 2-oxoglutarate and the 5-hydroxyectoine (and by inference ectoine) and their corresponding binding partners in the catalytic core of the ectoine hydroxylase becomes apparent (Fig. 8*A*). This network of interactions mediates the precise positioning of the ectoine substrate in such way that the C5 carbon atom in its pyrimidine ring can be hydroxylated in a stereo-specific manner. The ectoine hydroxylase catalyzes this enzyme reaction with high accuracy, both *in vivo* (33) and *in vitro* (27).

The EctD enzyme is not only of interest from an ecophysiological and biotechnological point of view (9, 10), it also has the potential for use in chemical biology with respect to the generation of chemically modified ectoine molecules. Synthetic ectoine derivatives with either expanded or reduced ring sizes have already been reported (70, 71), and these might lead to interesting novel biotechnological applications or medical uses (9, 10, 17). The architecture of the catalytic core of the ectoine hydroxylase (Fig. 7 and 8) is probably flexible enough to allow chemical modifications of these existing synthetic molecules. An EctD-mediated hydroxylation might endow them with novel stress-protective and structure-preserving functions in the same way that it allows 5-hydroxyectoine to function strikingly different from ectoine in alleviating desiccation stress (36).

The structural insight that we provide here for the active site of the EctD protein (Figs. 7 and 8) might therefore aid the rational chemical design of new ectoine derivatives that then could be hydroxylated either *in vivo* or *in vitro* by the EctD enzyme. Furthermore, our crystallographic study might also inspire experiments to improve the moderate catalytic efficiencies of ectoine hydroxylases (22) through targeted mutagenesis or *in vivo* evolution experiments to enhance their industrial use.

Acknowledgments—We thank Jochen Sohn for excellent technical assistance in the overproduction and purification of the EctD protein and Georg Lentzen and Irina Bagyan (bitop AG) for their kind gifts of ectoine and 5-hydroxyectoine. We thank the staff of the P13 and P14 beamlines at EMBL, Hamburg, Germany, for their kind support during crystal screening. We acknowledge the European Synchrotron Radiation Facility for provision of synchrotron radiation facilities (ID23eh2). We greatly appreciate the expert help of Vickie Koogle in the language editing of our manuscript and thank Lutz Schmitt for helpful discussions and the kind support for this project. E. B. greatly valued the hospitality of Tom Silhavy during a sabbatical at the Department of Molecular Biology, Princeton University (Princeton, NJ). N. W. and E. B. are very grateful to Rolf Thauer for his continued support.

REFERENCES

1. Yancey, P. H. (2005) Organic osmolytes as compatible, metabolic and counteracting cytoprotectants in high osmolarity and other stresses. *J. Exp. Biol.* **208,** 2819–2830
2. Kempf, B., and Bremer, E. (1998) Uptake and synthesis of compatible solutes as microbial stress responses to high osmolality environments. *Arch. Microbiol.* **170,** 319–330
3. Bremer, E., and Krämer, R. (2000) in *Bacterial Stress Responses* (Storz, G., and Hengge-Aronis, R., eds) pp. 79–97, American Society for Microbiology, Washington, D. C.
4. Street, T. O., Bolen, D. W., and Rose, G. D. (2006) A molecular mechanism for osmolyte-induced protein stability. *Proc. Natl. Acad. Sci. U.S.A.* **103,** 13997–14002
5. Ignatova, Z., and Gierasch, L. M. (2006) Inhibition of protein aggregation *in vitro* and *in vivo* by a natural osmoprotectant. *Proc. Natl. Acad. Sci. U.S.A.* **103,** 13357–13361
6. Bourot, S., Sire, O., Trautwetter, A., Touzé, T., Wu, L. F., Blanco, C., and Bernard, T. (2000) Glycine betaine-assisted protein folding in a *lysA* mutant of *Escherichia coli*. *J. Biol. Chem.* **275,** 1050–1056
7. Diamant, S., Eliahu, N., Rosenthal, D., and Goloubinoff, P. (2001) Chemical chaperones regulate molecular chaperones *in vitro* and in cells under combined salt and heat stresses. *J. Biol. Chem.* **276,** 39586–39591
8. Galinski, E. A., Pfeiffer, H. P., and Trüper, H. G. (1985) 1,4,5,6-Tetrahydro-2-methyl-4-pyrimidinecarboxylic acid. A novel cyclic amino acid from halophilic phototrophic bacteria of the genus *Ectothiorhodospira*. *Eur. J. Biochem.* **149,** 135–139
9. Lentzen, G., and Schwarz, T. (2006) Extremolytes: Natural compounds from extremophiles for versatile applications. *Appl. Microbiol. Biotechnol.* **72,** 623–634
10. Pastor, J. M., Salvador, M., Argandoña, M., Bernal, V., Reina-Bueno, M., Csonka, L. N., Iborra, J. L., Vargas, C., Nieto, J. J., and Cánovas, M. (2010) Ectoines in cell stress protection: uses and biotechnological production. *Biotechnol. Adv.* **28,** 782–801
11. Lippert, K., and Galinski, E. A. (1992) Enzyme stabilization by ectoine-type compatible solutes: protection against heating, freezing and drying. *Appl. Microbiol. Biotechnol.* **37,** 61–65
12. Knapp, S., Ladenstein, R., and Galinski, E. A. (1999) Extrinsic protein stabilization by the naturally occurring osmolytes β-hydroxyectoine and betaine. *Extremophiles* **3,** 191–198
13. Borges, N., Ramos, A., Raven, N. D., Sharp, R. J., and Santos, H. (2002) Comparative study of the thermostabilizing properties of mannosylglycerate and other compatible solutes on model enzymes. *Extremophiles* **6,** 209–216
14. Van-Thuoc, D., Hashim, S. O., Hatti-Kaul, R., and Mamo, G. (2013) Ecto-

ine-mediated protection of enzyme from the effect of pH and temperature stress: a study using *Bacillus halodurans* xylanase as a model. *Appl. Microbiol. Biotechnol.* **97,** 6271–6278
15. Manzanera, M., García de Castro, A., Tøndervik, A., Rayner-Brandes, M., Strøm, A. R., and Tunnacliffe, A. (2002) Hydroxyectoine is superior to trehalose for anhydrobiotic engineering of *Pseudomonas putida* KT2440. *Appl. Environ. Microbiol.* **68,** 4328–4333
16. Schwibbert, K., Marin-Sanguino, A., Bagyan, I., Heidrich, G., Lentzen, G., Seitz, H., Rampp, M., Schuster, S. C., Klenk, H. P., Pfeiffer, F., Oesterhelt, D., and Kunte, H. J. (2011) A blueprint of ectoine metabolism from the genome of the industrial producer *Halomonas elongata* DSM 2581 T. *Environ. Microbiol.* **13,** 1973–1994
17. Graf, R., Anzali, S., Buenger, J., Pfluecker, F., and Driller, H. (2008) The multifunctional role of ectoine as a natural cell protectant. *Clin. Dermatol.* **26,** 326–333
18. Becker, J., Schäfer, R., Kohlstedt, M., Harder, B. J., Borchert, N. S., Stöveken, N., Bremer, E., and Wittmann, C. (2013) Systems metabolic engineering of *Corynebacterium glutamicum* for production of the chemical chaperone ectoine. *Microb. Cell Fact.* **12,** 110
19. Marini, A., Reinelt, K., Krutmann, J., and Bilstein, A. (2014) Ectoine-containing cream in the treatment of mild to moderate atopic dermatitis: a randomised, comparator-controlled, intra-individual double-blind, multi-center trial. *Skin Pharmacol. Physiol.* **27,** 57–65
20. Abdel-Aziz, H., Wadie, W., Abdallah, D. M., Lentzen, G., and Khayyal, M. T. (2013) Novel effects of ectoine, a bacteria-derived natural tetrahydropyrimidine, in experimental colitis. *Phytomedicine* **20,** 585–591
21. Sun, H., Glasmacher, B., and Hofmann, N. (2012) Compatible solutes improve cryopreservation of human endothelial cells. *Cryo Lett.* **33,** 485–493
22. Widderich, N., Höppner, A., Pittelkow, M., Heider, J., Smits, S. H., and Bremer, E. (2014) Biochemical properties of ectoine hydroxylases from extremophiles and their wider taxonomic distribution among microorganisms. *PLoS One* **9,** e93809
23. Louis, P., and Galinski, E. A. (1997) Characterization of genes for the biosynthesis of the compatible solute ectoine from *Marinococcus halophilus* and osmoregulated expression in *Escherichia coli*. *Microbiology* **143,** 1141–1149
24. Kuhlmann, A. U., and Bremer, E. (2002) Osmotically regulated synthesis of the compatible solute ectoine in *Bacillus pasteurii* and related *Bacillus* spp. *Appl. Environ. Microbiol.* **68,** 772–783
25. Kuhlmann, A. U., Bursy, J., Gimpel, S., Hoffmann, T., and Bremer, E. (2008) Synthesis of the compatible solute ectoine in *Virgibacillus pantothenticus* is triggered by high salinity and low growth temperature. *Appl. Environ. Microbiol.* **74,** 4560–4563
26. Bursy, J., Kuhlmann, A. U., Pittelkow, M., Hartmann, H., Jebbar, M., Pierik, A. J., and Bremer, E. (2008) Synthesis and uptake of the compatible solutes ectoine and 5-hydroxyectoine by *Streptomyces coelicolor* A3(2) in response to salt and heat stresses. *Appl. Environ. Microbiol.* **74,** 7286–7296
27. Bursy, J., Pierik, A. J., Pica, N., and Bremer, E. (2007) Osmotically induced synthesis of the compatible solute hydroxyectoine is mediated by an evolutionarily conserved ectoine hydroxylase. *J. Biol. Chem.* **282,** 31147–31155
28. Saum, S. H., and Müller, V. (2008) Growth phase-dependent switch in osmolyte strategy in a moderate halophile: ectoine is a minor osmolyte but major stationary phase solute in *Halobacillus halophilus*. *Environ. Microbiol.* **10,** 716–726
29. Mustakhimov, I. I., Reshetnikov, A. S., Glukhov, A. S., Khmelenina, V. N., Kalyuzhnaya, M. G., and Trotsenko, Y. A. (2010) Identification and characterization of EctR1, a new transcriptional regulator of the ectoine biosynthesis genes in the halotolerant methanotroph *Methylomicrobium alcaliphilum* 20Z. *J. Bacteriol.* **192,** 410–417
30. García-Estepa, R., Argandoña, M., Reina-Bueno, M., Capote, N., Iglesias-Guerra, F., Nieto, J. J., and Vargas, C. (2006) The *ectD* gene, which is involved in the synthesis of the compatible solute hydroxyectoine, is essential for thermoprotection of the halophilic bacterium *Chromohalobacter salexigens*. *J. Bacteriol.* **188,** 3774–3784
31. Peters, P., Galinski, E. A., and Trüper, H. G. (1990) The biosyntheis of ectoine. *FEMS Microbiol. Lett.* **71,** 157–162
32. Ono, H., Sawada, K., Khunajakr, N., Tao, T., Yamamoto, M., Hiramoto, M., Shinmyo, A., Takano, M., and Murooka, Y. (1999) Characterization of biosynthetic enzymes for ectoine as a compatible solute in a moderately halophilic eubacterium, *Halomonas elongata*. *J. Bacteriol.* **181,** 91–99
33. Inbar, L., and Lapidot, A. (1988) The structure and biosynthesis of new tetrahydropyrimidine derivatives in actinomycin D producer *Streptomyces parvulus*. Use of ^{13}C- and ^{15}N-labeled L-glutamate and ^{13}C and ^{15}N NMR spectroscopy. *J. Biol. Chem.* **263,** 16014–16022
34. Prabhu, J., Schauwecker, F., Grammel, N., Keller, U., and Bernhard, M. (2004) Functional expression of the ectoine hydroxylase gene (*thpD*) from *Streptomyces chrysomallus* in *Halomonas elongata*. *Appl. Environ. Microbiol.* **70,** 3130–3132
35. Kurz, M. (2008) Compatible solute influence on nucleic acids: many questions but few answers. *Saline Systems* **4,** 6
36. Tanne, C., Golovina, E. A., Hoekstra, F. A., Meffert, A., and Galinski, E. A. (2014) Glass-forming property of hydroxyectoine is the cause of its superior function as a dessication protectant. *Front. Microbiol.* **5,** 150
37. Hausinger, R. P. (2004) FeII/α-ketoglutarate-dependent hydroxylases and related enzymes. *Crit. Rev. Biochem. Mol. Biol.* **39,** 21–68
38. Aik, W., McDonough, M. A., Thalhammer, A., Chowdhury, R., and Schofield, C. J. (2012) Role of the jelly-roll fold in substrate binding by 2-oxoglutarate oxygenases. *Curr. Opin. Struct. Biol.* **22,** 691–700
39. Hangasky, J. A., Taabazuing, C. Y., Valliere, M. A., and Knapp, M. J. (2013) Imposing function down a (cupin)-barrel: secondary structure and metal stereochemistry in the αKG-dependent oxygenases. *Metallomics* **5,** 287–301
40. Kundu, S. (2012) Distribution and prediction of catalytic domains in 2-oxoglutarate-dependent dioxygenases. *BMC Res. Notes* **5,** 410
41. Wong, S. D., Srnec, M., Matthews, M. L., Liu, L. V., Kwak, Y., Park, K., Bell, C. B., 3rd, Alp, E. E., Zhao, J., Yoda, Y., Kitao, S., Seto, M., Krebs, C., Bollinger, J. M., Jr., and Solomon, E. I. (2013) Elucidation of the Fe(IV)=O intermediate in the catalytic cycle of the halogenase SyrB2. *Nature* **499,** 320–323
42. Grzyska, P. K., Appelman, E. H., Hausinger, R. P., and Proshlyakov, D. A. (2010) Insight into the mechanism of an iron dioxygenase by resolution of steps following the FeIV=HO species. *Proc. Natl. Acad. Sci. U.S.A.* **107,** 3982–3987
43. Widderich, N., Pittelkow, M., Höppner, A., Mulnaes, D., Buckel, W., Gohlke, H., Smits, S. H., and Bremer, E. (2014) Molecular dynamics simulations and structure-guided mutagenesis provide insight into the architecture of the catalytic core of the ectoine hydroxylase. *J. Mol. Biol.* **426,** 586–600
44. Reuter, K., Pittelkow, M., Bursy, J., Heine, A., Craan, T., and Bremer, E. (2010) Synthesis of 5-hydroxyectoine from ectoine: crystal structure of the non-heme iron(II) and 2-oxoglutarate-dependent dioxygenase EctD. *PLoS One* **5,** e10647
45. Ting, L., Williams, T. J., Cowley, M. J., Lauro, F. M., Guilhaus, M., Raftery, M. J., and Cavicchioli, R. (2010) Cold adaptation in the marine bacterium, *Sphingopyxis alaskensis*, assessed using quantitative proteomics. *Environ. Microbiol.* **12,** 2658–2676
46. Hoeppner, A., Widderich, N., Bremer, E., and Smits, S. H. J. (2014) Overexpression, crystallization and preliminary X-ray crystallographic analysis of the ectoine hydroxylase from *Sphingopyxis alaskensis*. *Acta Crystallogr. F Struct. Biol. Crystalliz. Commun.* **70**, 493–496
47. Miller, J. H. (1972) *Experiments in Molecular Genetics*, Cold Spring Harbor Laboratory Press, Cold Spring Harbor, NY
48. Lovenberg, W., Buchanan, B. B., and Rabinowitz, J. C. (1963) Studies on the chemical nature of *Clostridial ferredoxin*. *J. Biol. Chem.* **238,** 3899–3913
49. Kabsch, W. (2010) XDS. *Acta Crystallogr. D Biol. Crystallogr.* **66,** 125–132
50. Kabsch, W. (2010) Integration, scaling, space-group assignment and post-refinement. *Acta Crystallogr. D Biol. Crystallogr.* **66,** 133–144
51. McCoy, A. J., Grosse-Kunstleve, R. W., Adams, P. D., Winn, M. D., Storoni, L. C., and Read, R. J. (2007) Phaser crystallographic software. *J. Appl. Crystallogr.* **40,** 658–674
52. Emsley, P., Lohkamp, B., Scott, W. G., and Cowtan, K. (2010) Features and development of Coot. *Acta Crystallogr. D Biol. Crystallogr.* **66,** 486–501
53. Murshudov, G. N., Vagin, A. A., and Dodson, E. J. (1997) Refinement of

macromolecular structures by the maximum-likelihood method. *Acta Crystallogr. D Biol. Crystallogr.* **53,** 240–255
54. Hoeppner, A., Schmitt, L., and Smits, S. H. (2013) in *Advances Topics on Crystal Growth* (Ferreira, S., ed) pp. 3–44, InTech Europe, Janeza Trdine 9, 51000 Rijeka, Croatia
55. McDonough, M. A., Kavanagh, K. L., Butler, D., Searls, T., Oppermann, U., and Schofield, C. J. (2005) Structure of human phytanoyl-CoA 2-hydroxylase identifies molecular mechanisms of Refsum disease. *J. Biol. Chem.* **280,** 41101–41110
56. Zhang, Z., Kochan, G. T., Ng, S. S., Kavanagh, K. L., Oppermann, U., Schofield, C. J., and McDonough, M. A. (2011) Crystal structure of PHYHD1A, a 2OG oxygenase related to phytanoyl-CoA hydroxylase. *Biochem. Biophys. Res. Commun.* **408,** 553–558
57. Blasiak, L. C., Vaillancourt, F. H., Walsh, C. T., and Drennan, C. L. (2006) Crystal structure of the non-haem iron halogenase SyrB2 in syringomycin biosynthesis. *Nature* **440,** 368–371
58. Wong, C., Fujimori, D. G., Walsh, C. T., and Drennan, C. L. (2009) Structural analysis of an open active site conformation of nonheme iron halogenase CytC3. *J. Am. Chem. Soc.* **131,** 4872–4879
59. Khare, D., Wang, B., Gu, L., Razelun, J., Sherman, D. H., Gerwick, W. H., Håkansson, K., and Smith, J. L. (2010) Conformational switch triggered by α-ketoglutarate in a halogenase of curacin A biosynthesis. *Proc. Natl. Acad. Sci. U.S.A.* **107,** 14099–14104
60. Strieker, M., Kopp, F., Mahlert, C., Essen, L. O., and Marahiel, M. A. (2007) Mechanistic and structural basis of stereospecific Cβ-hydroxylation in calcium-dependent antibiotic, a daptomycin-type lipopeptide. *ACS Chem. Biol.* **2,** 187–196
61. Helmetag, V., Samel, S. A., Thomas, M. G., Marahiel, M. A., and Essen, L. O. (2009) Structural basis for the erythro-stereospecificity of the L-arginine oxygenase VioC in viomycin biosynthesis. *FEBS J.* **276,** 3669–3682
62. Knauer, S. H., Hartl-Spiegelhauer, O., Schwarzinger, S., Hänzelmann, P., and Dobbek, H. (2012) The Fe(II)/α-ketoglutarate-dependent taurine dioxygenases from *Pseudomonas putida* and *Escherichia coli* are tetramers. *FEBS J.* **279,** 816–831
63. Krissinel, E., and Henrick, K. (2007) Inference of macromolecular assemblies from crystalline state. *J. Mol. Biol.* **372,** 774–797
64. Straganz, G. D., and Nidetzky, B. (2006) Variations of the 2-His-1-carboxylate theme in mononuclear non-heme FeII oxygenases. *Chembiochem* **10,** 1536–1548
65. Lecher, J., Pittelkow, M., Zobel, S., Bursy, J., Bönig, T., Smits, S. H., Schmitt, L., and Bremer, E. (2009) The crystal structure of UehA in complex with ectoine-A comparison with other TRAP-T binding proteins. *J. Mol. Biol.* **389,** 58–73
66. Hanekop, N., Höing, M., Sohn-Bösser, L., Jebbar, M., Schmitt, L., and Bremer, E. (2007) Crystal structure of the ligand-binding protein EhuB from *Sinorhizobium meliloti* reveals substrate recognition of the compatible solutes ectoine and hydroxyectoine. *J. Mol. Biol.* **374,** 1237–1250
67. Kuhlmann, S. I., Terwisscha van Scheltinga, A. C., Bienert, R., Kunte, H. J., and Ziegler, C. (2008) 1.55 A structure of the ectoine binding protein TeaA of the osmoregulated TRAP-transporter TeaABC from *Halomonas elongata*. *Biochemistry* **47,** 9475–9485
68. Inbar, L., Frolow, F., and Lapidot, A. (1993) The conformation of new tetrahydropyrimidine derivatives in solution and in the crystal. *Eur. J. Biochem.* **214,** 897–906
69. Stöveken, N., Pittelkow, M., Sinner, T., Jensen, R. A., Heider, J., and Bremer, E. (2011) A specialized aspartokinase enhances the biosynthesis of the osmoprotectants ectoine and hydroxyectoine in *Pseudomonas stutzeri* A1501. *J. Bacteriol.* **193,** 4456–4468
70. Schnoor, M., Voss, P., Cullen, P., Böking, T., Galla, H. J., Galinski, E. A., and Lorkowski, S. (2004) Characterization of the synthetic compatible solute homoectoine as a potent PCR enhancer. *Biochem. Biophys. Res. Commun.* **322,** 867–872
71. Witt, E. M., Davies, N. W., and Galinski, E. A. (2011) Unexpected property of ectoine synthase and its application for synthesis of the engineered compatible solute ADPC. *Appl. Microbiol. Biotechnol.* **91,** 113–122